IEEE Access
Multidisciplinary | Rapid Review | Open Access Journal

Received 17 July 2024, accepted 22 August 2024, date of publication 30 August 2024, date of current version 10 September 2024.

Digital Object Identifier 10.1109/ACCESS.2024.3452316

RESEARCH ARTICLE

Flexible Meta-Patch Rectenna Array for Energizing Low-Power Wearable Medical Sensors

HUSSEIN YAHYA ALKHALAF[1], MOHD YAZED AHMAD[1,2], (Member, IEEE), HARIKRISHNAN RAMIAH[2], (Senior Member, IEEE), A. K. M. ZAKIR HOSSAIN[3], (Member, IEEE), S. M. KAYSER AZAM[4], AND AUNG THIHA[5]

[1]Biosensor and Embedded System Laboratory, Department of Biomedical Engineering, Universiti Malaya, Kuala Lumpur 50603, Malaysia
[2]Analog, Digital and RF Research Group, Department of Electrical Engineering, Faculty of Engineering, Universiti Malaya, Kuala Lumpur 50603, Malaysia
[3]Centre for Telecommunication Research and Innovation (CeTRI), Fakulti Teknologi dan Kejuruteraan Elektronik dan Komputer, Universiti Teknikal Malaysia Melaka, Durian Tunggal, Melaka 76100, Malaysia
[4]Department of Electrical Engineering, Universiti Malaya, Kuala Lumpur 50603, Malaysia
[5]Centre for Innovation in Medical Engineering, Department of Biomedical Engineering, Universiti Malaya, Kuala Lumpur 50603, Malaysia

Corresponding author: Mohd Yazed Ahmad (myaz@um.edu.my)

This research was funded by the Ministry of Higher Education Malaysia via Fundamental Research Grant Scheme FRGS/1/2020/TK0/UM/02/45 (FP124-2020).

ABSTRACT This article presents a low-cost 2 × 2 metasurface-based rectenna array operating at the 2.45 GHz industrial, scientific, and medical (ISM) band, designed to power low-power wearable medical sensors (WMS). The proposed antenna is a novel textile-based metasurface interlayer patch (meta-patch) antenna fabricated on a felt fabric substrate, which replaces the conventional ground plane with a grounded metasurface consisting of a 3 × 3 unit cell array. A single excitation port is used for both the patch antenna and the metasurface to improve gain, efficiency, and bandwidth. The meta-patch antenna achieved a high gain of 7 dB, an efficiency of 77%, and an enhanced bandwidth of 120 MHz. The rectifier employs a seven-stage Cockcroft-Walton Voltage Multiplier (CWVM) topology, fabricated on a rigid substrate. To evaluate the performance of the meta-patch rectenna array and the effect of adding more elements, the proposed meta-patch rectenna was tested in single-element, 2 × 1 array, and 2 × 2 array configurations under continuous RF power. The single-element, 2 × 1 rectenna array, and 2 × 2 rectenna array achieved power conversion efficiencies (PCE) of 52%, 53%, and 56%, with DC output powers of 414 μW, 429 μW, and 450 μW, respectively, at an input power of -1 dBm. The results demonstrate the potential of the proposed rectenna arrays for efficiently energizing low-power WMS.

INDEX TERMS Cockcroft-Walton rectifier, meta-patch rectenna array, meta-patch textile antenna, metasurface-based antenna, RF energy harvesting, seven-stage rectifier, textile rectenna array, wearable rectenna array, wearable medical sensors.

I. INTRODUCTION

Wearable Medical Sensors (WMS) have garnered significant attention in recent years for their potential to revolutionize healthcare by enabling continuous monitoring and real-time data collection. These sensors play an important role in detecting physiological changes, biochemical variations, and motion, with a wide range of clinical applications [1]. They offer a promising alternative to current techniques for monitoring therapeutic drugs, which can be utilized in the management of chronic diseases. Additionally, these sensors are integral to the Industrial Internet of Medical Things (IoMT), supporting emerging biomedical applications by enhancing connectivity and providing data-driven insights [2].

The associate editor coordinating the review of this manuscript and approving it for publication was Photos Vryonides.

The current power source for WMS primarily relies on typical batteries, which may require frequent recharging or replacement. Despite recent advancements in battery technology resulting in the development of compact and high-capacity batteries, their operational lifespan remains relatively short [3]. Additionally, batteries may contain harmful or poisonous chemicals. In specific applications, such as implantable drug delivery systems, cardiac pacemakers, and microsensors reliant on batteries, patients may undergo additional and undesirable procedures, such as surgery, for sensor recharging [4], [5]. Consequently, to address these challenges, RF Energy Harvesting (RFEH) technology has emerged as an alternative power source for WMS. RFEH technology can effectively meet the power requirements of these sensors, which typically range from picowatts to microwatts [6].

Numerous textile RFEH rectennas and rectenna arrays have been developed to enable wearable RFEH systems. These systems utilize textile materials such as felt, jeans, cotton, organza fabric, Cordura fabric, and polyester as substrates for wearable antennas and rectifier circuits, thus forming fully textile rectennas and arrays [6], [7], [8], [9], [10]. For instance, Vital et al. [6] presented a 2×2 and 2×3 textile rectenna array operating at 2.45 GHz and embroidered on organza with conductive wires. The 2×3 rectenna array achieves a DC output power of 600 μW at 10 cm away from the RF source. Another fully textile rectenna array was introduced by Estrada et al. [7] consisting of 16 and 81 elements printed on a cotton T-shirt, operating at 2-5 GHz and achieving a DC output power of 32 μW at an incident power density of 4 μW/cm^2, with a power conversion efficiency (PCE) of 32% at 100 μW/cm^2. However, the PCE dropped to 17% at 14 μW/cm^2 power density at 2.9 GHz. Lopez et al. [8] developed a 2×2 pure textile rectenna array operating at 2.4-2.48 GHz, achieving a DC output power of 1.1 mW with a PCE of 31% at 12 dBm input power. Conversely, other studies have proposed combining textile antennas with PCB rectifiers for wearable RFEH systems [5], [11], [12], [13]. For instance, Adami et al. [13] presented a 2×1 wristband rectenna array based on a textile antenna fabricated on woven polyester and polyester felt substrate with a PCB rectifier fabricated on RT/duroid5880, achieving a maximum end-to-end efficiency of 28.7% at -7 dBm.

Moreover, several studies have utilized metasurfaces in the design of receiver antennas to enhance the overall performance of rectenna systems [14], [15], [16], [17], [18], [19]. Metasurfaces are artificial materials comprising unit cell array structures capable of manipulating electromagnetic waves at subwavelength propagation distances, enabling complex applications such as polarization transformation, generalized refraction, and signal multiplexing [20], [21]. The integration of metasurfaces in wearable antenna design enhances various antenna parameters, including gain [22], radiation characteristics [23], and bandwidth [24]. These unique properties render metasurfaces highly suitable for wearable RFEH systems, as they can significantly improve antenna performance. However, a common drawback in some related works that employed metasurfaces in wearable antenna design is the bulky size of the metasurface, which increases overall antenna dimensions [25].

The related literature highlights the pressing need for further enhancement in the design of wearable rectenna array systems. Many existing wearable rectenna arrays suffer from low PCE and low DC output power, making it impractical to supply sufficient power for certain WMS. Moreover, some studies have reported high DC output power at high input power levels, which is unrealistic, particularly in indoor environments with predictably low input power levels. Additionally, the utilization of lossy textile feedlines, antenna-to-rectifier interconnectors, and shorting vias contributes to additional power loss and increases fabrication complexity in rectenna systems. Therefore, ensuring the reliability and performance stability of rectenna systems is crucial for enabling more efficient wearable RFEH applications.

In this article, a textile-based metasurface interlayer patch (meta-patch) antenna integrated with a seven-stage Cockcroft-Walton Voltage Multiplier (CWVM) rectifier is proposed to form a meta-patch rectenna array system. The novel configuration of the proposed meta-patch antenna involves positioning the metasurface layer below the patch antenna substrate and above the ground plane, with both the patch antenna and the metasurface layer excited by a single excitation port. This configuration enhances the gain, efficiency, and bandwidth of the antenna, addressing the narrow bandwidth issue usually associated with traditional patch antennas. The proposed metasurface is designed to match the size of the patch antenna, overcoming the larger metasurface size issue found in some related works. On the rectifier side, a PCB seven-stage CWVM rectifier is presented to achieve high DC output power at low input power ranges. Although a rectifier with a rigid substrate is not ideal for wearable rectennas, the PCB rectifier provides reliable and stable performance at a low cost. After designing the antenna and rectifier circuit, 2×2 meta-patch rectenna arrays were fabricated and measured. To ensure flexibility, comfort, and avoid direct contact with the skin, the rectenna arrays are attached to a 2 mm thick surface of felt fabric within the clothing and organized to occupy minimal space. The proposed rectenna arrays have been tested in free space, on-body, and under realistic Wi-Fi conditions.

To the best of our knowledge and based on the literature conducted, this is the first article to present metasurface-based wearable rectenna arrays. The contributions of this work are as follows:

1) The design of a novel meta-patch antenna with high gain and efficiency, thereby improving the overall efficiency of rectenna arrays system.
2) Low-cost meta-patch rectenna arrays with high DC output power and efficiency compared to existing wearable rectenna arrays, particularly at low input power ranges.

Design, simulation, fabrication, and measurement results are presented in Sections II through IV.

II. META-PATCH ANTENNA DESIGN AND PRINCIPLES

A. METASURFACE DESIGN

To design the unit cell array of the metasurface, a felt fabric substrate with a thickness of 2 mm, a dielectric constant of 1.215, and a loss tangent of 0.016 at 2.45 GHz was used. These parameters were based on measurements conducted using an Agilent 85070E Dielectric Probe Kit. The choice of the substrate is due to its flexibility, comfort [26], durability, ease of fabrication [27], compatibility for wearable applications and cost-effectiveness. In this work, the primary goal of utilizing the metasurface unit cell is to achieve precise directional control of radiation by reflecting energy away from unintended paths. This approach aims to enhance radiation efficiency in the desired direction while minimizing the energy that penetrates the metasurface and interacts with surrounding tissues. Fig. 1 demonstrates the geometry of the proposed meta-patch antenna. Fig 1(c) shows the metasurface unit cell, which consists of a Split Ring Resonator (SRR) structure.

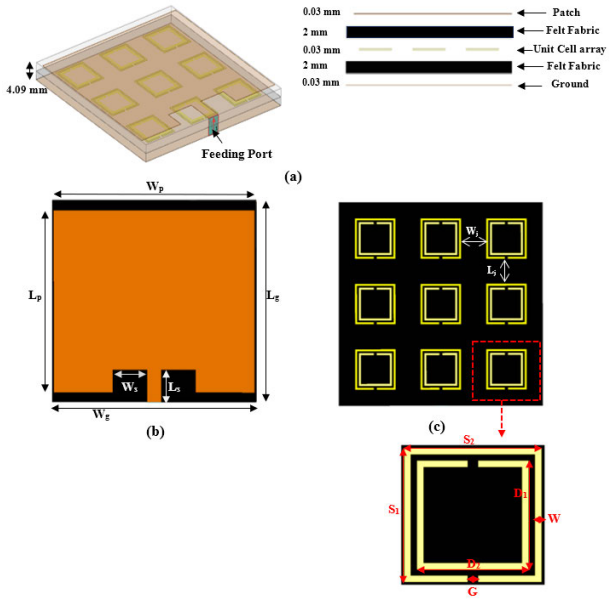

FIGURE 1. Geometry of the proposed meta-patch antenna: (a) side and 3D view of the proposed design (b) top view of the proposed antenna; (c) top view of the metasurface design with 3 × 3 unit cell array.

To determine the dimensions of the metasurface unit cell, the free space wavelength λ_o is calculated as follows [28]:

$$\lambda_o = \frac{c}{f} \tag{1}$$

where c represents the speed of light, f signifies the operating frequency. Subsequently, the effective wavelength (λ_{eff}) is calculated as follows:

$$\lambda_{eff} = \frac{\lambda o}{\sqrt{\epsilon r}} \tag{2}$$

TABLE 1. Optimized dimensions of the meta-patch antenna.

Parameter	Size (mm)
Lg	59
Wg	59
Lp	53.37
Wp	58.1
Ls	9.95
Ws	9.5
Wj	7.15
Lj	7.15
S_1	11.7
S_2	11.7
D_1	9.5
D_2	9.5
W	1.1
G	0.9

The dimensions of the metasurface unit cell are typically a fraction of the effective wavelength. The metasurface unit cell size is determined to be approximately $\lambda_{eff}/10$ to ensure that the metasurface behaves as a homogeneous medium and efficiently interacts with the electromagnetic waves [29], [30], [31]. The initial dimensions served as starting points for further optimization through the Ansys HFSS simulator [30]. The SRR structure parameters, such as outer length (S_1), outer width (S_2), inner length (D_1), inner width (D_2), ring width (W), and gap width (G) were iteratively optimized to achieve the desired performance at the targeted resonant frequency [31], [32]. The optimized dimensions of the metasurface unit cell and the antenna are listed in Table 1.

The defining ports and boundary conditions of the metasurface unit cell are shown in Fig. 2(a). Waveguide ports excite the unit cell with an electromagnetic wave and measure transmitted and reflected signals along the Y-direction. Periodic boundary conditions are implemented by applying a Perfect Electric Conductor (PEC) boundary along the X-direction and a Perfect Magnetic Conductor (PMC) boundary along the Z-direction [33].

Generally, the absorption rate of the material $A(\omega)$ will be determined using the reflection rate $R(\omega) = |S_{11}|^2$ and transmission rate $T(\omega) = |S_{21}|^2$ as follow [34]:

$$A(\omega) = 1 - R(\omega) - T(\omega) \tag{3}$$

Fig. 2(a) illustrates the transmission and reflection coefficients of the proposed metasurface unit cell. The results indicate that the metasurface exhibits strong reflective properties, making it well-suited for integration with the proposed antenna, which operates at 2.45 GHz.

The functioning of the metasurface can be determined by calculating its effective permittivity (ϵ) and effective permeability (μ) as given in 4 and 5 [35]:

$$\varepsilon(\omega) = Re(\varepsilon) + jIm(\varepsilon) \tag{4}$$

$$\mu(\omega) = Re(\mu) + jIm(\mu) \tag{5}$$

In this case, the negative refractive index of the material is identified in real terms, while the material losses are represented by the imaginary parts. The effective parameters

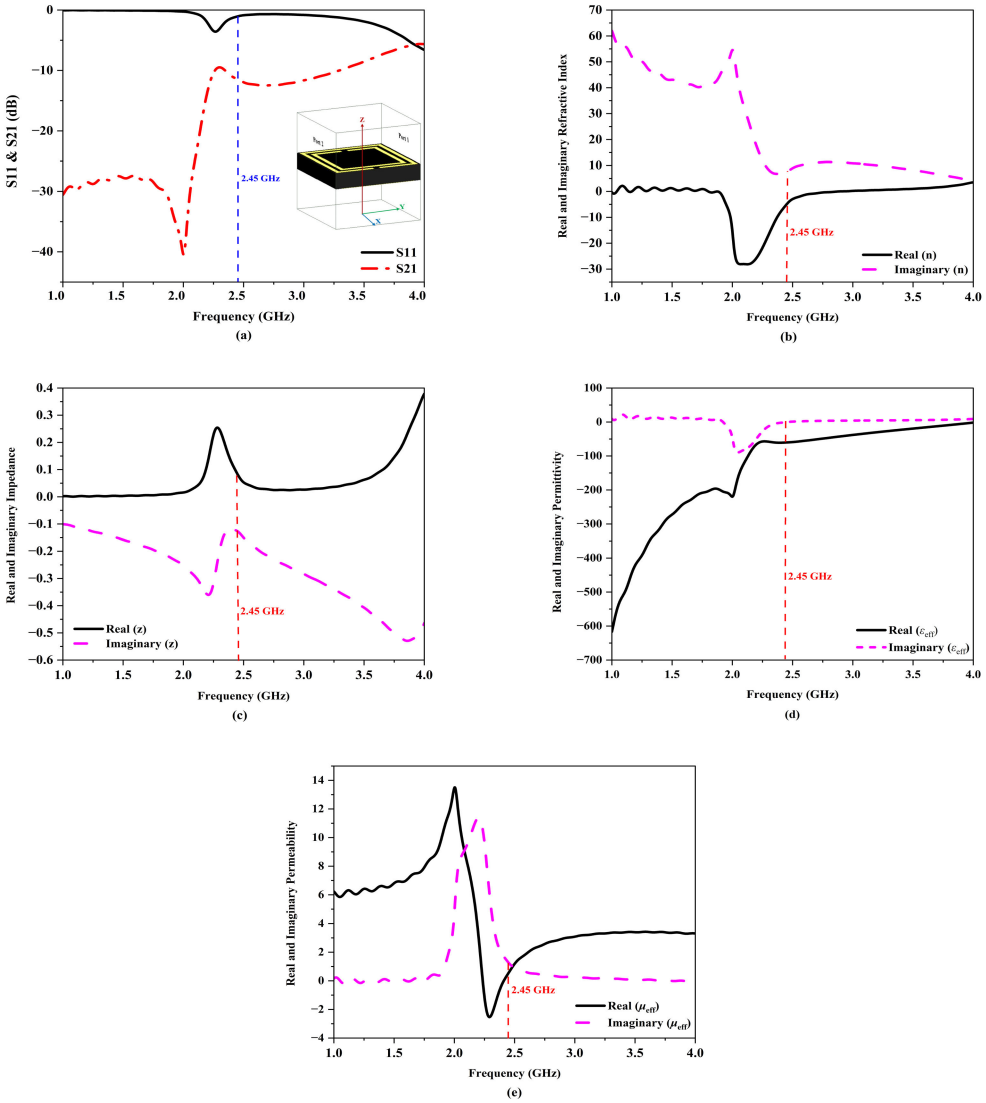

FIGURE 2. Performance analysis of the metasurface unit cell; (a) reflection coefficient (S_{11}) and transmission coefficient (S_{21}) of the metasurface unit cell; (b) the real and imaginary parts of the refractive index (n); (c) the real and imaginary parts of the impedance (z); (d) the real and imaginary parts of the effective permittivity (ϵ_{eff}); (f) the real and imaginary part of the effective permeability (μ_{eff}).

were obtained utilizing the S-parameters retrieval method. The refractive index (n), impedance (z), along with effective permittivity (ϵ_{eff}), and permeability (μ_{eff}) are derived using MATLAB according to [33].

Fig. 2(b) shows the refractive index (n) of the metasurface unit cell. In the frequency range of 2.0 - 3.0 GHz, the real part of the refractive index is negative, indicating that the proposed metasurface unit cell achieves a negative refractive index within this range, including the desired frequency band. This negative refractive index is a characteristic property of the metasurface, which manipulates electromagnetic waves in a manner that reflects the energy in the opposite direction.

Fig. 2(c) depicts the impedance (z) of the metasurface unit cell. From this figure, it can be observed that the real part of the impedance is positive at the desired frequency band, indicating that it exhibits balanced resistance to wave propagation, which ensures effective interaction with incident waves. This balance is vital for the metasurface to efficiently reflect waves. Moreover, the imaginary part of the impedance is negative, indicating the capacitive behavior of the metasurface. This capacitive behavior assists in phase shifting and achieving the desired reflection properties.

Fig. 2(d) shows the effective permittivity (ϵ_{eff}) of the metasurface unit cell. At the desired frequency band of 2.45 GHz, the real part of the effective permittivity is negative, demonstrating the capability of the proposed metasurface to reflect rather than transmit or absorb electromagnetic waves.

The imaginary part of the permittivity remains close to zero, indicating minimal loss within the material.

Fig. 2(e) presents the effective permeability (μ_{eff}) of the metasurface unit cell. The real part of the permeability is near zero at the 2.45 GHz frequency band, indicating resonant behavior. Additionally, the imaginary part of the permeability is around zero at this frequency, indicating minimal loss. These characteristics emphasize the effectiveness of the metasurface in redirecting incoming energy and minimizing absorption by the human body.

B. DESIGN AND FABRICATION OF THE META-PATCH TEXTILE ANTENNA

Due to their small size, low profile, and ease of integration, rectangular patch antennas find widespread application in various wearable devices, including wearable RF energy harvesters. However, these antennas often encounter challenges such as high losses, limited control over radiation patterns, and restricted communication ranges [36]. This work introduces an innovative technique to enhance the performance of rectangular patch antennas by replacing the conventional ground plane with a grounded metasurface and utilizing a single excitation port for both the patch antenna and the metasurface. The proposed configuration aims to increase gain, enable precise control over the radiation pattern for enhanced directivity, and improve bandwidth. The single excitation port simplifies the system's design, resulting in a more compact configuration suitable for wearable energy harvesting applications.

The metasurface is designed to match the size of the patch antenna, comprising a 3 × 3 metasurface unit cell array with an SRR structure. The proposed antenna is designed with overall dimensions of 59 × 59 × 4.09 mm^3 as shown in Fig. 1(a) and Fig. 1(b), operating at ISM band of 2.45 GHz. The patch is constructed from copper with a thickness of 0.03 mm, and its dimensions (length Lp and width Wp) are specified. The substrate for the patch antenna is the same as that of the metasurface unit cell array, with an identical thickness. For optimal impedance matching, the feedline width (Wf), slot length (Ls), and slot width (Ws) are carefully evaluated.

A 3 × 3 metasurface unit cell array with an SRR structure, made of copper with a thickness of 0.03 mm, is attached to the felt fabric substrate using glue. The amount of glue has been carefully controlled to minimize its impact on the proposed antenna's performance. The fabrication of the metasurface unit cell involves the use of photolithography technique. While the photolithography process is well-known, we aim to elaborate on how we utilized this technique to manually attach a metasurface unit cell with an SRR structure to a textile substrate, which presents some challenges. The steps for fabricating the proposed metasurface unit cell array are illustrated in Fig. 3 and are outlined as follows:

1) **Cleaning:** The copper sheet was cleaned with acetone and isopropanol, then affixed to the Pressure-Sensitive Adhesive (PSA) layer to support the copper, ensuring that no bubbles were present.
2) **Applying Photosensitive Dry Film:** The Photosensitive Dry Film (PDF) was cut to the same size as the copper layer. The first protective layer was then removed, and the film was carefully attached to the (copper + PSA) layers.
3) **Lamination:** Dry film lamination was performed 2-3 times using an office paper laminator.
4) **Exposure:** The sample, with the photomask attached to a fully transparent film, was placed in the ultraviolet (UV) exposure unit for 60 seconds and then removed.
5) **Heating Oven:** The second protective layer of the photoresist was removed, and the printed sample was placed in a heating oven for approximately 5 minutes.
6) **Developing:** A PCB developer solution was diluted with water in a 1:3 ratio. The sample was then immersed in the solution for 30-40 seconds to remove the photoresist.
7) **Etching:** The sample was submerged in a ferric chloride etching solution for approximately 30 minutes to remove the copper.
8) **Stripping:** The printed sample was immersed in sodium hydroxide (NaOH) to remove the remaining photoresist on the copper. Subsequently, the second adhesive layer of PSA was removed from the sample, and it was attached to the felt fabric substrate with a small amount of glue.

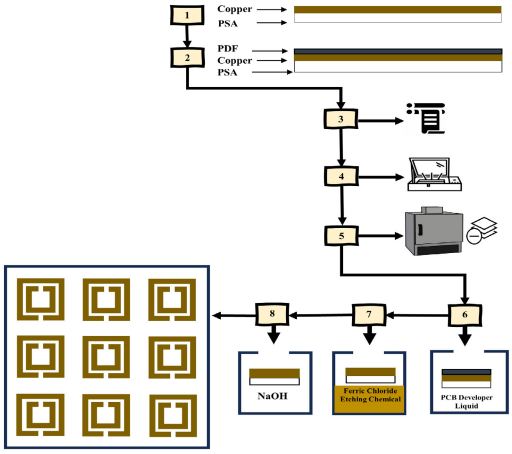

FIGURE 3. Fabrication steps of the metasurface unit cell array using Photolithography technique.

The fabricated prototype of the proposed meta-patch antenna is depicted in Fig. 4.

C. PERFORMANCE ANALYSIS OF THE META-PATCH ANTENNA

1) ANALYSIS OF THE REFLECTION COEFFICIENT

The overall effect of using the metasurface in the design of the proposed antenna is illustrated in Table. 2.

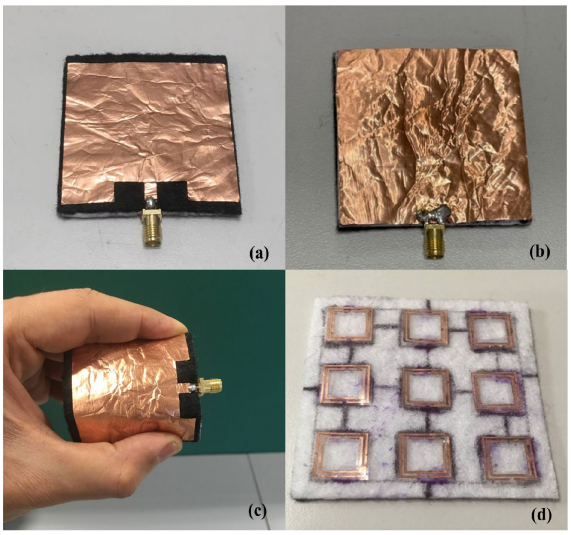

FIGURE 4. Fabricated prototypes of the meta-patch antenna; (a) front view; (b) back view; (c) its flexibility; (d) the metasurface plane.

TABLE 2. Performance comparison for the proposed antenna with and without metasurface.

Performance Metrics	Patch Antenna	Meta-Patch Antenna
Peak gain (dB)	5.6	8.7
Radiation Efficiency (%)	43	79
Frequency (GHz)	2.52	2.43
Bandwidth range (GHz)	2.49-2.53	2.38-2.5
Reflection Coefficient (dB)	-11.9	-22.3

Fig. 5 demonstrates the simulated and measured reflection coefficient (S_{11}) results for the meta-patch antenna in different environments: free space and a body phantom model compared with the reference patch antenna in free space. The proposed antenna is designed primarily for use on the back of the body, where it is expected to encounter minimal bending or twisting. Therefore, the evaluation did not include testing on curved surfaces. Measurements were conducted using a Rohde & Schwarz ZVB4 Vector Network Analyzer (VNA). The results show that the proposed meta-patch antenna exhibits a better reflection coefficient and a slight shift in frequency toward the desired frequency band. This shift is attributed to the presence of the metasurface, which introduces new electromagnetic properties, significantly enhancing the bandwidth from 38.1 MHz to 120 MHz compared to the reference patch antenna. The measured results demonstrated good agreement with the simulated results, both on and off the body, indicating the excellent performance of the proposed meta-patch antenna in different environments.

2) ANALYSIS OF THE GAIN AND RADIATION PATTERN

Fig. 6 illustrates the measurement setup for the proposed meta-patch antenna in an anechoic chamber. In Fig. 6(a), the actual front and back views of the antenna tested in this environment are depicted. Fig. 6(b) presents a comparison of the measured gain and efficiency against the frequency of the meta-patch antenna, showing high gain (7 dB) and efficiency (77%) achieved by the antenna.

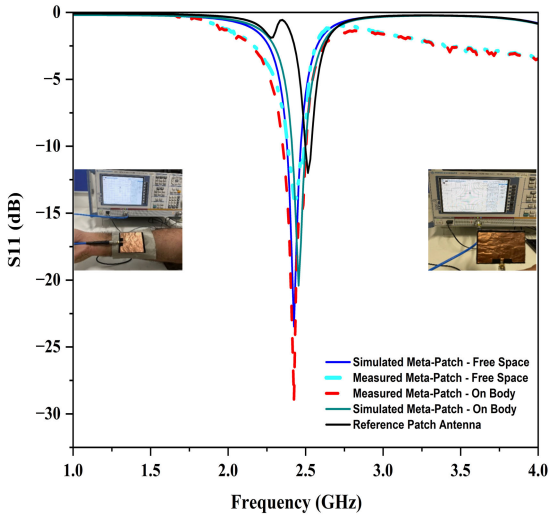

FIGURE 5. Simulated and measured reflection coefficient of the meta-patch antenna in free space and on the body with the reference patch antenna in free space.

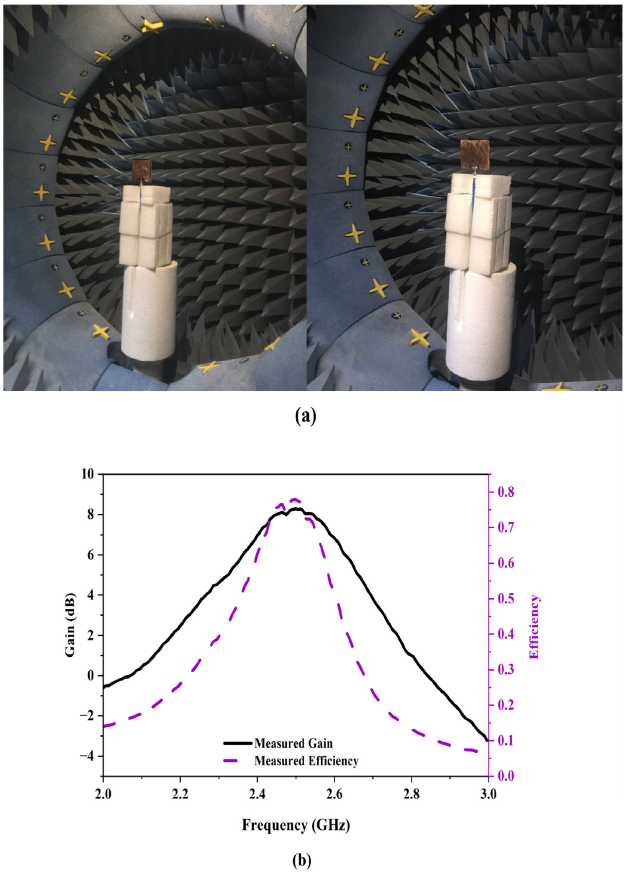

FIGURE 6. Measurement setup for the proposed meta-patch antenna in an anechoic chamber; (a) actual setup of the antenna undergoing measurements; (b) measured gain and efficiency versus frequency for the meta-patch antenna.

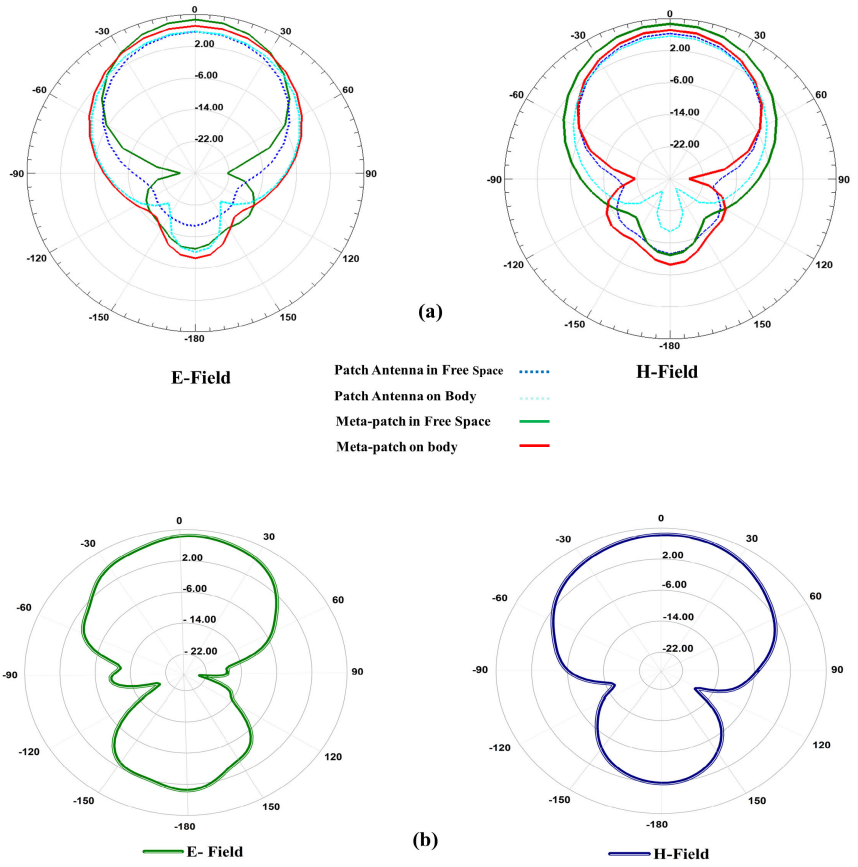

FIGURE 7. Simulated and measured radiation patterns of the proposed antenna; (a) Simulated radiation patterns for the meta-patch antenna and conventional patch antenna in free space and on the body at E-field and H-field; (b) Measured radiation pattern for the meta-patch antenna using an anechoic chamber.

Fig. 7 demonstrates the simulated and measured radiation patterns of the proposed antenna. Fig. 7(a) displays the simulated radiation patterns of the proposed meta-patch antenna and a reference patch antenna in free space and on the body, in both the E-field and H-field. The meta-patch antenna achieved high gains of 8.7 dB and 6.4 dB in free space and on-body, respectively, at 2.45 GHz, while the reference patch antenna exhibited lower gains of 5.6 dB and 5.7 dB in similar conditions. Furthermore, Fig. 7(b) depicts the measurement of the radiation pattern utilizing an anechoic chamber. The simulated and measured radiation pattern results of the proposed meta-patch antenna are shown to be in good agreement.

The outcomes indicate that the proposed meta-patch antenna is well-suited for RFEH applications, and capable of efficiently capturing energy from RF signals in its anticipated direction. Its directional characteristics help in blocking unwanted signals, thereby improving signal quality. This aligns with the usage patterns of wearable applications, enabling them to capture more power from identified RF sources such as Wi-Fi networks. Furthermore, the high gain and concentrated reception of the proposed antenna reduces interference, ensuring a stable and reliable power supply, making it suitable for efficient RFEH.

3) ANALYSIS OF THE SPECIFIC ABSORPTION RATE

Specific Absorption Rate (SAR) measures the average power absorbed by the body or tissue when exposed to an RF electromagnetic field, expressed in watts per kilogram (W/kg) [37]. The SAR value is calculated using the following equation:

$$SAR = \frac{\sigma |E|^2}{\rho} \tag{6}$$

where σ represents the conductivity of the tissue in siemens per meter (S/m), ρ signifies the tissue's mass density in kilograms per cubic meter (Kg/m^3), and E is defined as the Root Mean Square (RMS) of the electric field strength measured in volts per meter (V/m). According to the guidelines set by the International Commission on Non-Ionizing Radiation Protection (ICNIRP) and the American National Standards Institute (ANSI), the SAR value should not exceed 1.6 W/kg absorbed per 1 g of tissue or 2 W/kg absorbed per 10 g of tissue, respectively [38].

TABLE 3. Thickness and electrical properties of body phantom layers [40].

Body Phantom Layer	Thickness (mm)	εr	σ (S/m)
Skin	2	37.95	1.49
Fat	5	5.27	0.11
Muscle	20	52.67	1.77
Bone	13	18.49	0.82

Flexible patch antennas, due to their close proximity to the human body and reduced front-to-back ratio, may exhibit elevated SAR values compared to rigid counterparts. This is attributed to increased emission of undesirable radiation towards the body [39]. In this work, the metasurface plays a crucial role in mitigating this issue by redirecting energy away from the body, thus reducing the amount of energy absorbed. To evaluate the SAR value, the meta-patch antenna was positioned on a human body phantom composed of skin, fat, muscle, and bone layers, each separated by a 5 mm gap. The thickness and electrical properties of these layers are detailed in Table 3. Fig. 8 illustrates the simulated SAR value of the proposed meta-patch antenna. The meta-patch antenna demonstrated a low SAR value of 0.5202 W/kg, well below the standard limit of 1.6 W/Kg. This adherence to safety standards highlights the suitability of the meta-patch antenna for wearable applications, ensuring electromagnetic radiation exposure remains within acceptable limits when in proximity to the human body.

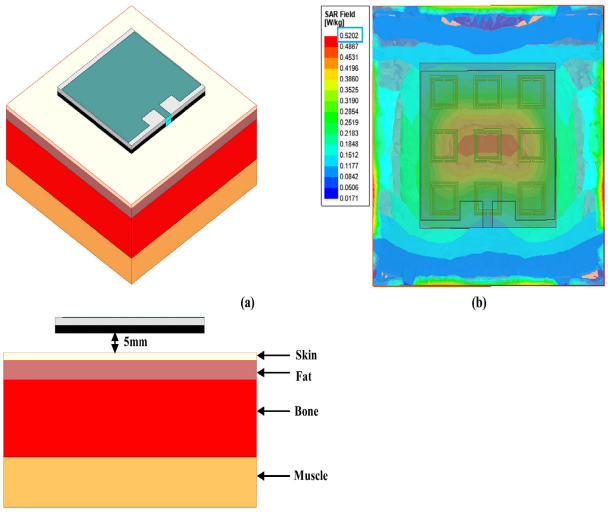

FIGURE 8. Measurement of SAR for the proposed meta-patch antenna; (a) schematic representation of the meta-patch antenna placed on the body phantom with a 5 mm gap; (b) simulated SAR of the meta-patch antenna.

4) COMPARISON OF PRIOR WORKS ON METAMATERIAL-BASED ANTENNAS

A performance comparison between the proposed meta-patch antenna and other state-of-the-art metamaterial-based (MTM) flexible antennas from the literature is presented in Table 4. The comparative analysis highlights the notable advantages exhibited by the meta-patch antenna. The proposed meta-patch antenna outperforms most flexible MTM-based antennas in terms of both gain and efficiency, despite its compact size. Although the work in [41] reports higher gain and efficiency, it is important to note that these results are associated with larger antenna dimensions.

III. DESIGN OF SEVEN-STAGE CWVM RECTIFIER

The ambient RF energy in the indoor environments is usually available in low power density, which range from −60 dBm to −20 dBm, therefore designing a rectifier circuit able to obtain a high output power from low input power range is essential to provide sufficient power for energizing the different WMS. In this work, a seven stage CWVM has been designed to achieve this purpose. The decision to use seven stages in the voltage multiplier circuit was primarily influenced by the escalating parasitic effects of each capacitor stage, resulting in cumulative losses that ultimately reduce the voltage gain [47], [48], [49]. The role of diodes is fundamental in designing the rectifier circuit as the sensitivity of the rectifier depends directly on the diode used. According to [50] the SMS7630 Schottky diode from Skyworks is the best to be used for rectification and impedance in RFEH systems. This diode provides several advantages for use in RFEH, such as low forward voltage drops, fast switching speed, high-frequency operation, cost effectiveness, surface-mountability, low capacitance, and small series resistance [51]. Hence, we have selected the SMS 7630 Schottky diode for this design.

The Harmonic Balance (HB) solver in the Advanced Design System (ADS) simulator software was utilized to simulate the seven-stage CWVM rectifier, and the nonlinear SPICE model of the Schottky diode was employed during the simulation. Additionally, co-simulation was performed in ADS Momentum to encompass the impact of the layout on the circuit's performance. Murata capacitors were utilized in the co-simulation to accurately emulate realistic performance.

Fig. 9(a) shows the schematic of the proposed seven-stage CWVM rectifier, which includes an L-shaped Impedance Matching Network (IMN) to to ensure matching with 50 Ω, a seven-stage voltage multiplier circuit, a filter capacitor, and a load resistance. The proposed rectifier is optimized to operate in the same frequency band as the proposed meta-patch antenna. The optimized design parameters for the proposed rectifier circuit are outlined in Table 5.

The layout of the seven-stage CWVM rectifier circuit is shown in Fig. 9(b). The trace length and width were specifically chosen to optimize the performance of the rectifier. These trace dimensions ensure minimal resistive losses and maintain impedance matching. The specific trace dimensions were determined through iterative simulations and optimizations using ADS to achieve the best performance in terms of efficiency and output power under the given operating conditions.

TABLE 4. Comparison of prior works on MTM-based flexible antennas.

Reference	Flexible Antenna	Dimensions (mm)	Frequency (GHz)	Substrate	Efficiency (%)	Gain (dB)	SAR (W/Kg)
[42]	Tapered Ring Monopole antenna with High-Impedance Surfaces (HIS)	87× 87	1.8	Arlon AD250	NA	5.25	0.113
[43]	Reconfigurable antenna integrated with Artificial Magnetic Conductor (AMC)	89 × 83	2.45	Rogers RO3003	NA	6.4	0.29
[44]	MTM-based fabric Antenna	60 × 60	2.4	Jeans	71	5.64	0.028
[41]	Flexible antenna backed with Frequency Selective Surface (FSS)	120 × 120	2.45	Jeans	80	7.78	0.164
[45]	Flexible dual-band antenna with a MTM structure	72 × 72	2.45,5.8	Polyimide	61.3	5.2	2.48
[25]	Flexible PDMS antenna with Metasurface	50 × 45	2.4	PDMS	68.06	2.88	1.52
[46]	Compact textile antenna based on a Metasurface	44.1 × 44.1	2.45,5.8	Felt Fabric	34	-0.69	0.476
This Work	**Textile Meta-patch Antenna**	**59 × 59**	**2.45**	**Felt Fabric**	**77**	**7**	**0.5202**

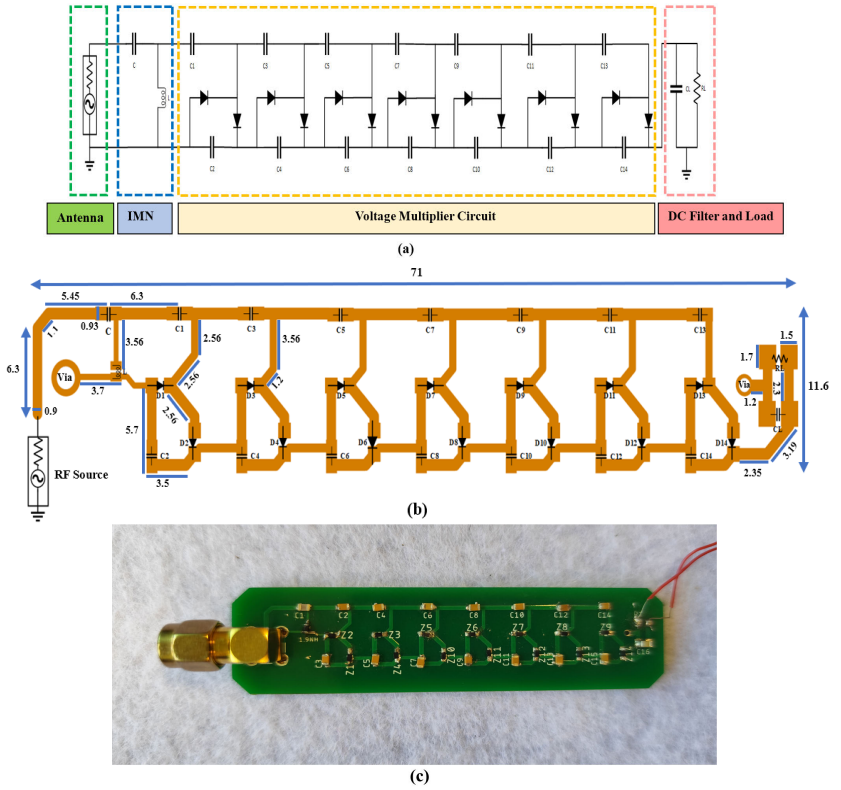

FIGURE 9. CWVM rectifier design and fabrication; (a) schematic of the seven-stage CWVM rectifier circuit; (b) layout of the proposed rectifier(dimensions in mm); (c) actual figure of the fabricated rectifier circuit prototype.

TABLE 5. Lumped component values mounted on the proposed rectifier.

Parameters	Values
L	1.8 nH
C	1 pF
C1-C14	56 pF
CL	1 µF
RL	50 KΩ

The actual figure of the fabricated prototype of the seven-stage CWVM rectifier circuit is shown in Fig. 9(c). The rectifier was fabricated on an FR4 substrate, which has a dielectric constant of 4.5, a loss tangent of 0.02, and a thickness of 1.6 mm.

A. PERFORMANCE ANALYSIS OF SEVEN-STAGE CWVM RECTIFIER

To verify the performance of the proposed rectifier before incorporating it with the meta-patch antenna, a seven-stage CWVM rectifier was fabricated and tested independently. The simulated and measured results of the proposed rectifier's reflection coefficient are illustrated in Fig. 10.

Visualizing the rectifier's wideband performance within a specific frequency band remains quite challenging due to the significant variation in impedance caused by dependent variables [48]. The measured result shows that the proposed rectifier achieved a wide bandwidth from 2.2 GHz to 2.8 GHz, making it well-suited for RFEH at the desired frequency band. VNA was used as a signal generator to inject the proposed rectifier with the RF signal at 2.45 GHz. A digital oscilloscope was employed to measure the DC output voltage at the output load resistance.

Fig. 11. presents a comparison between the simulated and measured DC output voltage as well as output power across different input power levels for the proposed rectifier. The proposed rectifier exhibited simulated and measured DC output voltages of 3.77 V and 3.18 V, respectively, at an input power of 0 dBm. Correspondingly, the simulated and measured output powers were 282 μW and 202 μW, indicating the performance of the rectifier under different input power environments.

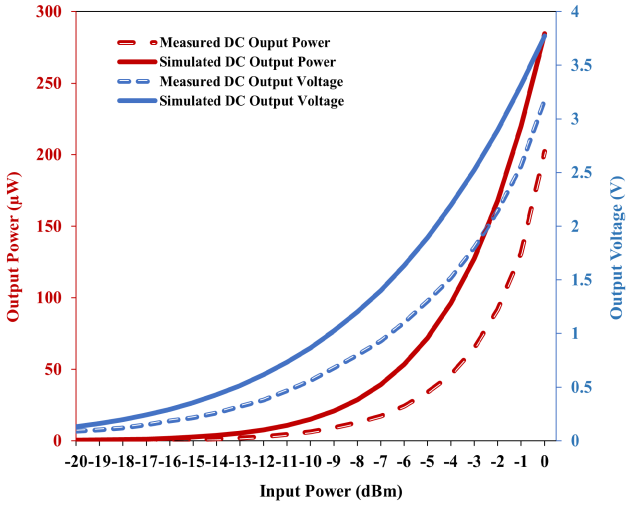

FIGURE 11. Simulated and measured DC output power and voltage of the CWVM rectifier circuit at various input power levels.

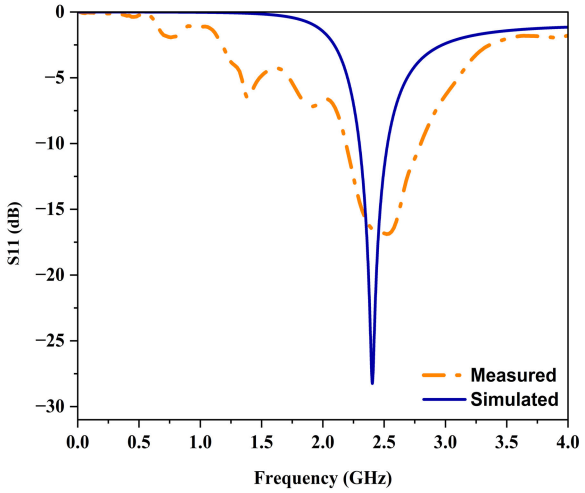

FIGURE 10. Simulated and measured reflection coefficient of the proposed CWVM rectifier.

In Fig. 12. the simulated and measured PCE of the seven-stage CWVM rectifier is illustrated. The PCE of the seven-stage CWVM rectifier is computed as follow:

$$PCE(\%) = \frac{V_{DC}^2}{P_{in} \times R_L} \times 100 \tag{7}$$

where V_{DC} represents the measured DC output voltage across the load resistance, R_L refers to the output load resistance, and P_{in} is the input RF power supplied to the rectifier circuit. The proposed rectifier achieved a simulated PCE of 28.45% and a measured PCE of 20.22% at an input power of 0 dBm with a load resistance of 50 kΩ. The measured results of the proposed rectifier may not fully replicate the conditions under which the rectifier operates in the rectenna system. Factors such as impedance matching, cable lengths, and other variables could affect the rectifier's performance when attached directly to the VNA. However, the overall PCE of the system increased significantly when the rectifier was integrated with the meta-patch antenna, forming the meta-patch rectenna system, as demonstrated in the subsequent performance analysis section.

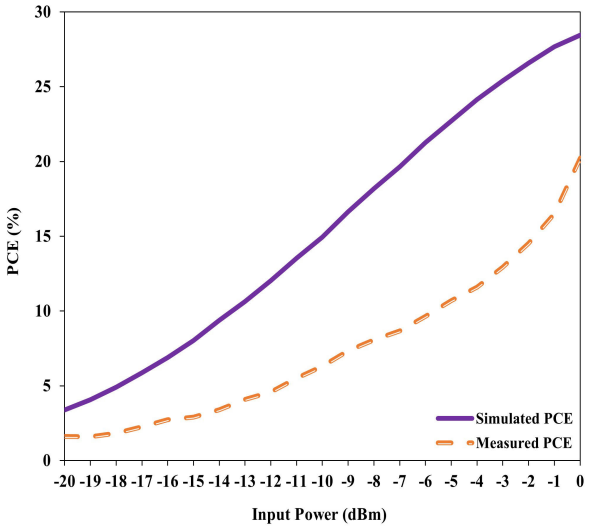

FIGURE 12. Simulated and measured PCE of the proposed seven-stage CWVM rectifier.

IV. PERFORMANCE ANALYSIS OF THE META-PATCH RECTENNA ARRAY

The integration of the proposed meta-patch antennas with seven-stage CWVM rectifiers formed a 2 × 2 meta-patch rectenna array, as illustrated in Fig. 13. The antennas were attached to the rectifiers using male and female SMA connectors. Although the use of SMA connectors might affect the wearability of the rectenna array, the choice of SMA connectors was due to their low-loss characteristics and reliability. To ensure flexibility and cohesion within

the rectenna array, the array was attached to a 2 mm thick felt fabric layer. Each antenna within the 2 × 2 meta-patch rectenna array is positioned opposite the others, with a gap distance of 2.5 cm between each rectenna to prevent mutual coupling effects and impedance mismatch. Additionally, this configuration minimizes the space occupied by the rectenna array. The overall dimensions of the proposed 2 × 2 meta-patch rectenna array measure 15.5 cm × 23.25 cm. The meta-patch rectenna array is connected in series to achieve a high DC output voltage.

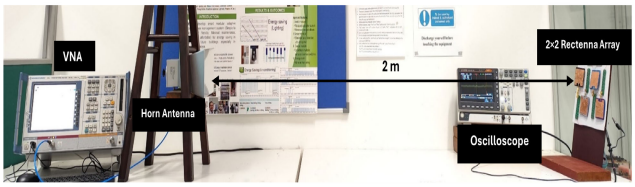

FIGURE 13. Experimental setup for the proposed meta-patch rectenna array.

To assess how the performance of the meta-patch rectenna array is influenced by increasing the number of rectenna elements, an experiment was conducted involving a single meta-patch rectenna element, a 2 × 1 meta-patch rectenna array, and a 2 × 2 meta-patch rectenna array, all subjected to continuous wave RF power. An examination was carried out to determine how varying the input power level affected the DC output voltage and DC output power. The experimental setup for testing and evaluating the DC output voltage at the terminals of the output load resistance is depicted in Fig. 13. A VNA is used to transmit the RF signal through a horn antenna with an 18 dBi gain at 2.45 GHz. The meta-patch rectenna array is connected to an oscilloscope to measure the DC output voltage. To ensure that the experiment remains within the far-field region of the transmission and receiving antennas, the proposed meta-patch rectenna array is positioned 2 meters away from the horn antenna.

Fig. 14 illustrates the DC output power of a single element rectenna at different input power levels. The proposed rectenna achieved a DC output power of 414 μW at −1 dBm input power and a load resistance of 50 kΩ. Fig. 15 demonstrates a comparison of the PCE of a single element, 2 × 1, and 2 × 2 meta-patch rectenna versus various input power levels. The single-element meta-patch rectenna achieved a maximum PCE of 52% at −1 dBm and a load resistance of 50 kΩ. The results of the single-element meta-patch rectenna demonstrate a significant improvement compared to testing the rectifier alone. This enhancement can be attributed to several factors, such as the integration of the rectifier with the meta-patch textile antenna, significantly enhancing the capture of RF energy from the RF source, due to its high efficiency, gain, and directivity.

Fig. 16 depicts the measurement of DC output power of the 2 × 1 meta-patch rectenna array at different input power levels. The proposed 2 × 1 meta-patch rectenna array

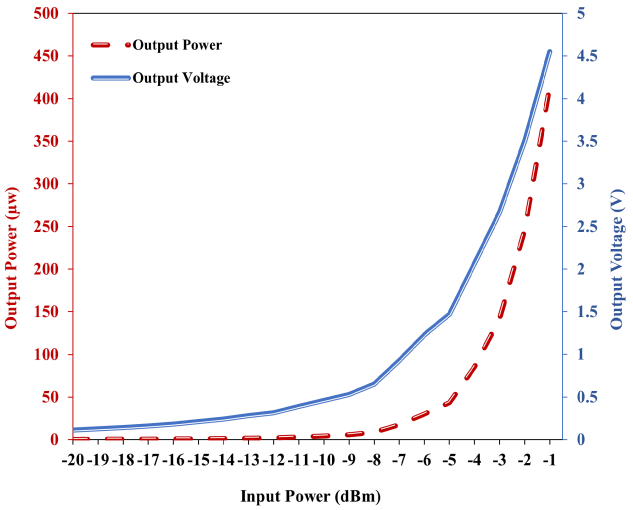

FIGURE 14. Performance of a single-element meta-patch rectenna: DC output voltage and power at various input power levels.

exhibited a DC output power of 429 μW at an input power of −1 dBm. Thus, we can observe that the DC output power increased by 15 μW compared to the single rectenna element at the same input power level. The maximum PCE of the 2 × 1 meta-patch rectenna array increased slightly compared to the single element achieving 53 % at −1 dBm and a load resistance of 100 kΩ, as shown in Fig. 15.

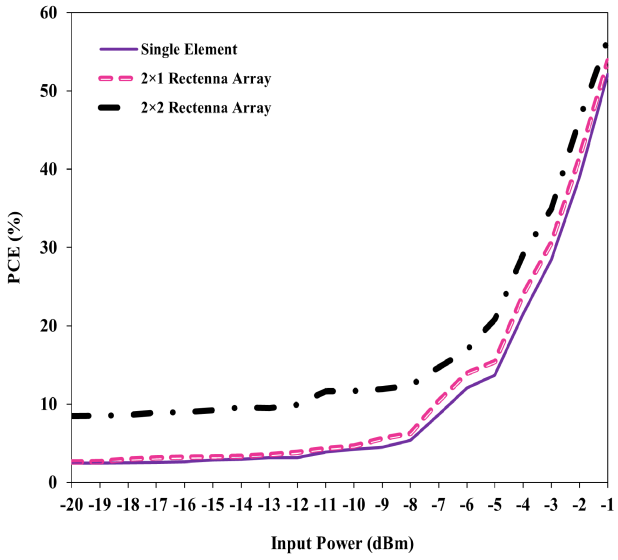

FIGURE 15. Comparison of the PCE of single element, 2 × 1, and 2 × 2 meta-patch rectennas.

Subsequently, a 2 × 2 meta-patch rectenna array is tested at different power levels. The DC output power of the proposed 2 × 2 meta-patch rectenna array was 450 μW recording an increment by 21 μW compared to the 2 × 1 meta-patch rectenna array and 36 μW compared to the single rectenna element at an input power of −1 dBm, as demonstrated in Fig. 17. The proposed 2 × 2 meta-patch rectenna array

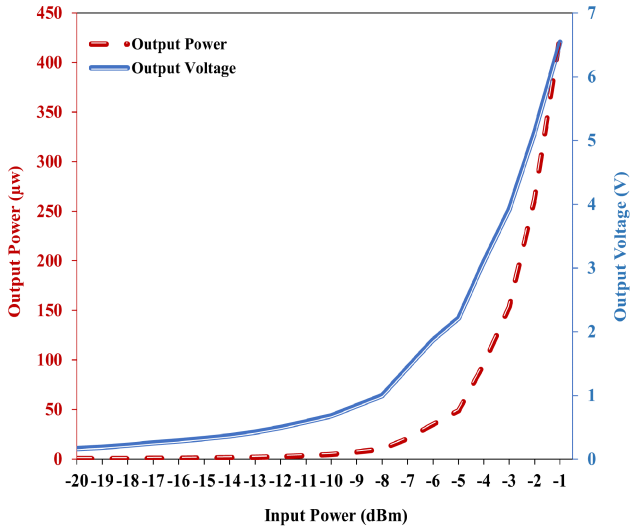

FIGURE 16. Performance of 2 × 1 meta-patch rectenna: DC output voltage and power at various input power levels.

exhibited higher efficiency than single element and 2 × 1 rectenna array achieving a 56% at −1 dBm and a load resistance of 200 kΩ., as depicted in Fig. 15. The observed increase in PCE when progressing from a single element to a 2 × 2 array can be attributed to several factors: the 2 × 2 array's higher gain and improved directivity capture more RF energy, resulting in greater effective input power for rectification. Additionally, enhanced impedance matching and reduced reactive losses contribute to more efficient power transfer.

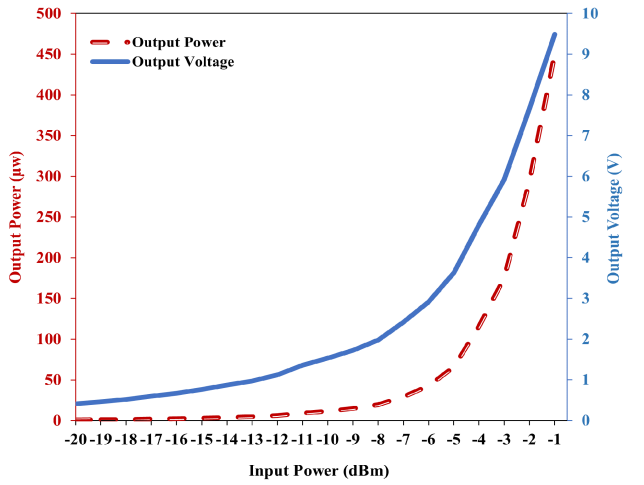

FIGURE 17. Performance of 2 × 2 meta-patch rectenna: DC output voltage and power at various input power levels.

The results show that the proposed meta-patch rectenna, whether as a single element, 2 × 1 rectennas, or 2 × 2 rectenna array, achieved a sufficient amount of power with good PCE at low input power levels, making it suitable for efficiently energizing wide range of low-power WMS.

A. META-PATCH RECTENNA ARRAY MEASUREMENTS ON HUMAN BODY

On-body tests were conducted to assess wearability, comfort, and to understand how the dielectric properties and movement patterns of the body affect the performance of the 2 × 2 meta-patch rectenna array. Fig. 18 illustrates the DC output voltage and power of the rectenna array placed on the human body at different input power levels. The proposed 2 × 2 meta-patch rectenna array achieved a maximum DC output power of 366.3 μW at an input power of −1 dBm and a load resistance of 200 kΩ. The maximum PCE of the rectenna array was 46% under similar conditions, as demonstrated in Fig. 19. These results indicate a minor deterioration in performance compared to the results in free space due to slight absorption and reflection of RF energy by human tissues.

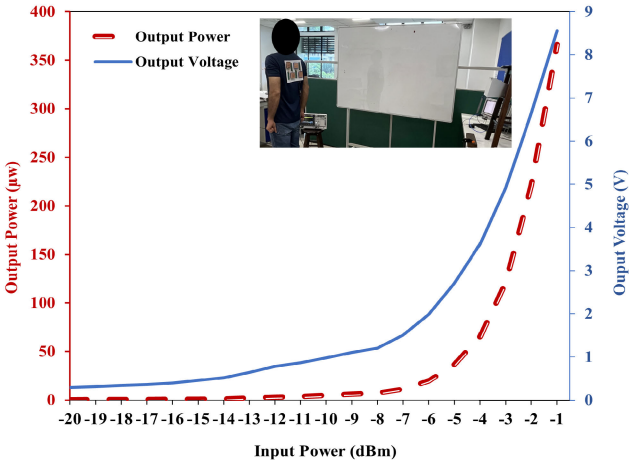

FIGURE 18. Performance of the proposed 2 × 2 meta-patch rectenna array on the human body: Measured DC output power and voltage versus various input power levels.

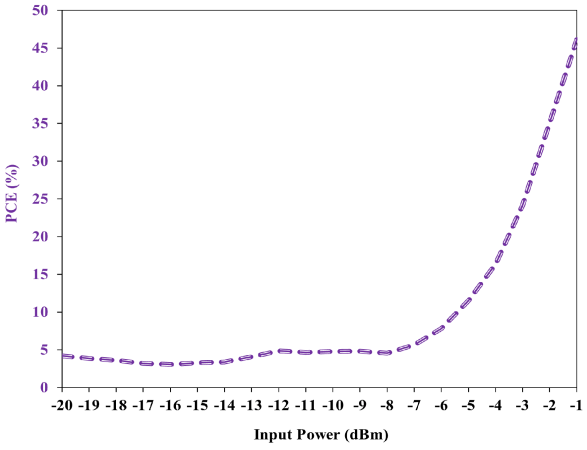

FIGURE 19. PCE of the proposed 2 × 2 meta-patch rectenna array on the human body.

To evaluate the performance of the rectenna array in realistic indoor environments where Wi-Fi signals are typi-

TABLE 6. Comparison of related work on wearable rectenna arrays.

Reference	Wearable Rectenna	Frequency (GHz)	Substrate	Rectifier Topology	Diode	Number of Array Element	Maximum DC output Power (µW)	PCE (%)
[13]	Textile antenna with PCB rectifier	2.45	Antenna: Woven Polyester and Polyester Felt Rectifier:RT/Duroid 5880	Single	SMS7630	2×1	150 at -5 dBm	28.7
[7]	Textile Rectenna	2-5	Cotton	Single	SMS7630	81-element array	32 at 4 $\mu W/cm^2$	32
[9]	Textile Rectenna	2.45	Cordura fabric	Single-stage full-wave Greinacher rectifier	HSMS-2862	2×2	NA	NA
[6]	Textile Rectenna	2.45	Antenna:Orgenza Rectifier: Stabilizer cloth	Single	SMS7630	2×2	70 at 500 µW	NA
[8]	Textile Rectenna	2.4-2.48	Felt	Voltage Doubler	SMS7630	2×2	1200 at 12 dBm	38
This Work	**Textile antenna with PCB rectifier**	**2.45**	**Antenna : Felt Fabric Rectifier : FR4**	**Seven Stage CWVM**	**SMS7630**	**2×2**	**450 at -1 dBm**	**56**

cally present, tests were conducted under Wi-Fi conditions. Fig. 20 shows the DC output power and voltage at varying distances from the router (ASUS AC3100). The rectenna array achieved a maximum DC output power of 102.1 μW at a distance of 10 cm from the router. The results highlight the impact of human body properties on rectenna array performance and its behavior under Wi-Fi conditions. Although a slight decline in performance was observed compared to free-space conditions, the rectenna array still demonstrated significant potential for efficient energy harvesting, particularly in realistic indoor environments.

Table 6 provides a comparison of the proposed meta-patch rectenna array with related works on flexible rectenna arrays for wearable applications. Notably, this study introduces the first MTM-based wearable rectenna array system. Compared to existing literature, the proposed rectenna array achieves high DC output power and PCE at low input power ranges. It is noteworthy that the measurements in this study were conducted without the use of a voltage booster attached to the rectenna, which have been commonly employed in experiments of many wearable rectenna systems and can significantly impact measurement results. The measured results of the proposed rectenna array, both on and off the body and under continuous RF wave or Wi-Fi conditions, show promising potential for efficiently powering numerous low-power WMS.

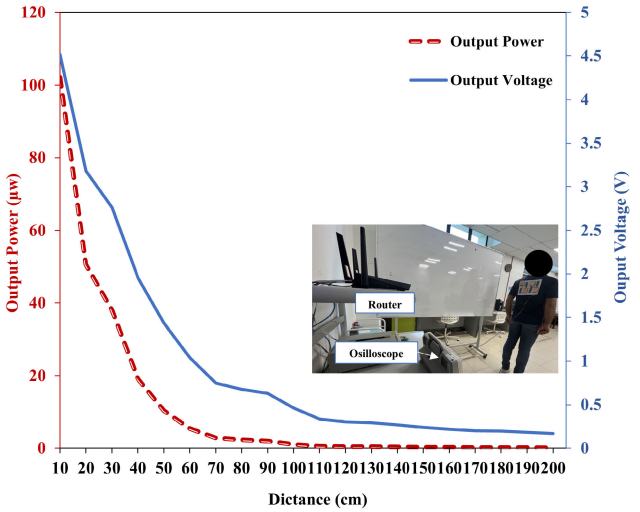

FIGURE 20. Performance of the 2 × 2 meta-patch rectenna array under Wi-Fi conditions: DC output power and voltage at varying distances from the router.

B. POTENTIAL WEARABLE MEDICAL APPLICATIONS

The power consumption of WMS is a critical factor that affects their performance and usability. It depends on several factors, including the type of sensor, data processing capabilities, communication protocols, and the efficiency of power management strategies. Some WMS with low power consumption include temperature sensors (113 pW and 1.4 μW) [52], [53], [54], [55], [56], cardiac activity sensors (0.3 μW) [57], electrocardiogram (ECG) amplifier sensors (2.76 μ W) [58], electronic-nose sensors (250 μW) [59], and other low power consumption biosensors with power requirement ranging from 9.3 nW to 436 μW [60], [61], [62].

The proposed meta-patch rectenna array, available in single-element, 2 × 1, and 2 × 2 configurations, with a DC output power range of 1 to 450 μW, promises to supply adequate power for numerous low-power WMS. Future plans involve integrating a power management unit (PMU) with the meta-patch rectenna array to optimize energy conversion and storage. This integration offers an alternative power source, enhancing the efficiency of energy harvesting and management.

The adoption of the meta-patch rectenna array as a power solution for wearable medical applications could further improve healthcare technologies, offering reliable and sustainable power generation. By effectively generating power and integrating PMU functionality, the proposed rectenna array system has the potential to significantly enhance

the performance and usability of various WMS, thereby improving patient care and healthcare system effectiveness.

V. CONCLUSION

The design, development, and evaluation of the metasurface-based flexible rectenna array system are presented in this article. The proposed meta-patch antenna, with high gain and efficiency, enhances the overall performance of the rectenna array system when integrated with a seven-stage CWVM rectifier designed for efficient operation in low input power ranges. The 2×2 meta-patch rectenna configuration achieved a PCE of 56% with a DC output power of 450 μW at an input power of -1 dBm. The ability of the rectifier to obtain high DC output power even at low input power levels is a key feature that enhances the overall effectiveness of the proposed rectenna system. Additionally, the 2×2 meta-patch rectenna array was tested on the human body to assess its wearability, achieving a PCE of 46% with a DC output power of 366.3 μW at -1 dBm input power. Furthermore, the 2×2 meta-patch rectenna array was evaluated in realistic indoor environments under Wi-Fi conditions. At a distance of 10 cm from the router, the proposed 2×2 meta-patch rectenna array exhibited a DC output power of 102.1 μW. These findings indicate that the meta-patch rectenna array system is capable of supplying sufficient power for a wide range of WMS. Future work involves further optimization of the proposed rectenna array and its integration with various WMS.

REFERENCES

[1] G. Rong, Y. Zheng, and M. Sawan, "Energy solutions for wearable sensors: A review," *Sensors*, vol. 21, no. 11, p. 3806, May 2021.

[2] S. A. A. Shah, I. A. Shah, S. Hayat, and H. Yoo, "Ultra-miniaturized implantable antenna enabling multiband operation for diverse industrial IoMT devices," *IEEE Trans. Antennas Propag.*, vol. 72, no. 2, pp. 1352–1362, Feb. 2024.

[3] H. Yahya Alkhalaf, M. Yazed Ahmad, and H. Ramiah, "Self-sustainable biomedical devices powered by RF energy: A review," *Sensors*, vol. 22, no. 17, p. 6371, Aug. 2022.

[4] J. Huang, Y. Zhou, Z. Ning, and H. Gharavi, "Wireless power transfer and energy harvesting: Current status and future prospects," *IEEE Wireless Commun.*, vol. 26, no. 4, pp. 163–169, Aug. 2019.

[5] Z. Chen, C. Song, J. Zhang, X. Zheng, V. Volskiy, P. Chu, and G. A. E. Vandenbosch, "Wearable rectenna with integrated miniaturized feeding slot and rectifier structure," *IEEE Trans. Antennas Propag.*, vol. 71, no. 5, pp. 3868–3881, May 2023.

[6] D. Vital, S. Bhardwaj, and J. L. Volakis, "Textile-based large area RF-power harvesting system for wearable applications," *IEEE Trans. Antennas Propag.*, vol. 68, no. 3, pp. 2323–2331, Mar. 2020.

[7] J. Antonio Estrada, E. Kwiatkowski, A. López-Yela, M. Borgoñós-García, D. Segovia-Vargas, T. Barton, and Z. Popovic, "RF-harvesting tightly coupled rectenna array tee-shirt with greater than octave bandwidth," *IEEE Trans. Microw. Theory Techn.*, vol. 68, no. 9, pp. 3908–3919, Sep. 2020.

[8] J.-M. Lopez-Garde, R. Del-Rio-Ruiz, J. Legarda, and H. Rogier, "2×2 textile rectenna array with electromagnetically coupled microstrip patch antennas in the 2.4 GHz WiFi band," *Electronics*, vol. 10, no. 12, p. 1447, Jun. 2021.

[9] Y.-J. Chi, C.-H. Lin, and C.-W. Chiu, "Design and modeling of a wearable textile rectenna array implemented on cordura fabric for batteryless applications," *J. Electromagn. Waves Appl.*, vol. 34, no. 13, pp. 1782–1796, Sep. 2020.

[10] I. Ullah, A. Komolafe, M. Wagih, and S. Beeby, "Flexible RF-power harvesting system for smart bandages using a textile dipole antenna array," in *Proc. 17th Eur. Conf. Antennas Propag. (EuCAP)*, Mar. 2023, pp. 1–4.

[11] M. Wagih, A. S. Weddell, and S. Beeby, "Omnidirectional dual-polarized low-profile textile rectenna with over 50% efficiency for sub-μW/cm^2 wearable power harvesting," *IEEE Trans. Antennas Propag.*, vol. 69, no. 5, pp. 2522–2536, May 2021.

[12] M. Wagih, A. S. Weddell, and S. Beeby, "Powering e-textiles using a single thread radio frequency energy harvesting rectenna," *Proceedings*, vol. 68, no. 1, p. 16, 2021.

[13] S.-E. Adami, P. Proynov, G. S. Hilton, G. Yang, C. Zhang, D. Zhu, Y. Li, S. P. Beeby, I. J. Craddock, and B. H. Stark, "A flexible 2.45-GHz power harvesting wristband with net system output from -24.3 dBm of RF power," *IEEE Trans. Microw. Theory Techn.*, vol. 66, no. 1, pp. 380–395, Jan. 2018.

[14] T. A. Elwi, "A further realization of a flexible metamaterial-based antenna on nickel oxide polymerized palm fiber substrates for RF energy harvesting," *Wireless Pers. Commun.*, vol. 115, no. 2, pp. 1623–1634, Nov. 2020.

[15] W. Lee, S.-I. Choi, H.-I. Kim, S. Hwang, S. Jeon, and Y.-K. Yoon, "Metamaterial-integrated high-gain rectenna for RF sensing and energy harvesting applications," *Sensors*, vol. 21, no. 19, p. 6580, Oct. 2021.

[16] M. A. Aldhaeebi and T. S. Almoneef, "Highly efficient planar metasurface rectenna," *IEEE Access*, vol. 8, pp. 214019–214029, 2020.

[17] A. Contreras and B. Rodríguez, "Optimization of a novel rectenna for RF energy harvesting at 2.45 GHz," *Wireless Pers. Commun.*, vol. 119, no. 3, pp. 2451–2467, Aug. 2021.

[18] M. E. Badawe and O. M. Ramahi, "Efficient metasurface rectenna for electromagnetic wireless power transfer and energy harvesting," *Prog. Electromagn. Res.*, vol. 161, pp. 35–40, 2018.

[19] I. A. Shah, M. Zada, S. A. A. Shah, A. Basir, and H. Yoo, "Flexible metasurface-coupled efficient wireless power transfer system for implantable devices," *IEEE Trans. Microw. Theory Techn.*, vol. 72, no. 4, pp. 2534–2547, Apr. 2024.

[20] N. Yu, P. Genevet, F. Aieta, M. A. Kats, R. Blanchard, G. Aoust, J.-P. Tetienne, Z. Gaburro, and F. Capasso, "Flat optics: Controlling wavefronts with optical antenna metasurfaces," *IEEE J. Sel. Topics Quantum Electron.*, vol. 19, no. 3, May 2013, Art. no. 4700423.

[21] M. A. Kats, R. Blanchard, P. Genevet, and F. Capasso, "Nanometre optical coatings based on strong interference effects in highly absorbing media," *Nature Mater.*, vol. 12, no. 1, pp. 20–24, Jan. 2013.

[22] G. K. Das, S. Basu, B. Mandal, D. Mitra, R. Augustine, and M. Mitra, "Gain-enhancement technique for wearable patch antenna using grounded metamaterial," *IET Microw., Antennas Propag.*, vol. 14, no. 15, pp. 2045–2052, Dec. 2020.

[23] Y. B. Chaouche, M. Nedil, M. Olaimat, M. E. Badawe, and O. M. Ramahi, "Wearable metasurface antenna based on electrically-small ring resonators for WBAN applications," *Electron. Lett.*, vol. 58, no. 1, pp. 4–7, Jan. 2022.

[24] H. A. Muhammad, Y. I. Abdulkarim, P. A. Abdoul, and J. Dong, "Textile and metasurface integrated wide-band wearable antenna for wireless body area network applications," *Int. J. Electron. Commun.*, vol. 169, Sep. 2023, Art. no. 154759.

[25] D. K. Janapala, M. Nesasudha, T. M. Neebha, and R. Kumar, "Specific absorption rate reduction using metasurface unit cell for flexible polydimethylsiloxane antenna for 2.4 GHz wearable applications," *Int. J. RF Microw. Comput.-Aided Eng.*, vol. 29, no. 9, Sep. 2019, Art. no. e21835.

[26] S. Shokeen, H. Singh, and A. Sharma, "An insight to textile substrates for wearable antenna," in *Proc. 6th ICMETE*, 2022, pp. 465–480.

[27] V. Marterer, M. Radouchová, R. Soukup, S. Hipp, and T. Blecha, "Wearable textile antennas: Investigation on material variants, fabrication methods, design and application," *Fashion Textiles*, vol. 11, no. 1, p. 9, Feb. 2024.

[28] D. M. Pozar, *Microwave Engineering*, 4th ed., Hoboken, NJ, USA: Wiley, 2011.

[29] C. Caloz and T. Itoh, *Electromagnetic Metamaterials: Transmission Line Theory and Microwave Applications*. Hoboken, NJ, USA: Wiley, 2006.

[30] N. Engheta and R. W. Ziolkowski, *Metamaterials: Physics and Engineering Explorations*. Hoboken, NJ, USA: Wiley, 2006.

[31] D. R. Smith and N. Kroll, "Negative refractive index in left-handed materials," *Phys. Rev. Lett.*, vol. 85, no. 14, pp. 2933–2936, Oct. 2000.

[32] J. B. Pendry, A. J. Holden, D. J. Robbins, and W. J. Stewart, "Magnetism from conductors and enhanced nonlinear phenomena," *IEEE Trans. Microw. Theory Techn.*, vol. 47, no. 11, pp. 2075–2084, Jun. 1999.

[33] A. B. Numan and M. S. Sharawi, "Extraction of material parameters for metamaterials using a full-wave simulator [education column]," *IEEE Antennas Propag. Mag.*, vol. 55, no. 5, pp. 202–211, Oct. 2013.

[34] M. Yoo, H. K. Kim, and S. Lim, "Angular- and polarization-insensitive metamaterial absorber using subwavelength unit cell in multilayer technology," *IEEE Antennas Wireless Propag. Lett.*, vol. 15, pp. 414–417, 2016.
[35] D. R. Smith, S. Schultz, P. Markos, and C. M. Soukoulis, "Determination of effective permittivity and permeability of metamaterials from reflection and transmission coefficients," *Phys. Rev. B*, vol. 65, no. 19, Apr. 2002, Art. no. 195104.
[36] R. Gonzalo, P. De Maagt, and M. Sorolla, "Enhanced patch-antenna performance by suppressing surface waves using photonic-bandgap substrates," *IEEE Trans. Microw. Theory Techn.*, vol. 47, no. 11, pp. 2131–2138, Jun. 1999.
[37] A. Kaur, H. Malik, V. Tanwar, K. Lamba, N. Kumar, and S. Sharma, "Effect of permittivity and conductivity of tissue on specific absorption rate of electromagnetic radiations," *Int. J. Innov. Technol. Exploring Eng. (IJITEE)*, vol. 1, no. 6, pp. 20–22, 2012.
[38] A. Afridi, S. Ullah, S. Khan, A. Ahmed, A. H. Khalil, and M. A. Tarar, "Design of dual band wearable antenna using metamaterials," *J. Microw. Power Electromagn. Energy*, vol. 47, no. 2, pp. 126–137, Jan. 2013.
[39] S. Nithya, V. Seethalakshmi, G. Vetrichelvi, M. Singaram, R. Prabhu, and S. Agarwal, "Investigation on performance characteristics of wearable textile patch antenna," in *Tracts in Electrical and Electronics Engineering*. Cham, Switzerland: Springer, 2023, pp. 47–58.
[40] M. A. Stuchly and S. S. Stuchly, "Dielectric properties of biological substances—Tabulated," *J. Microw. Power*, vol. 15, no. 1, pp. 19–25, Jan. 1980.
[41] B. Sugumaran, R. Balasubramanian, and S. K. Palaniswamy, "Reduced specific absorption rate compact flexible monopole antenna system for smart wearable wireless communications," *Eng. Sci. Technol., Int. J.*, vol. 24, no. 3, pp. 682–693, Jun. 2021.
[42] A. Kamalaveni and M. Ganesh Madhan, "A compact TRM antenna with high impedance surface for SAR reduction at 1800 MHz," *Int. J. Electron. Commun.*, vol. 70, no. 9, pp. 1192–1198, Sep. 2016.
[43] S. M. Saeed, C. A. Balanis, C. R. Birtcher, A. C. Durgun, and H. N. Shaman, "Wearable flexible reconfigurable antenna integrated with artificial magnetic conductor," *IEEE Antennas Wireless Propag. Lett.*, vol. 16, pp. 2396–2399, 2017.
[44] A. Y. I. Ashyap, Z. Z. Abidin, S. H. Dahlan, H. A. Majid, and G. Saleh, "Metamaterial inspired fabric antenna for wearable applications," *Int. J. RF Microw. Comput.-Aided Eng.*, vol. 29, no. 3, Mar. 2019, Art. no. e21640.
[45] M. Wang, Z. Yang, J. Wu, J. Bao, J. Liu, L. Cai, T. Dang, H. Zheng, and E. Li, "Investigation of SAR reduction using flexible antenna with metamaterial structure in wireless body area network," *IEEE Trans. Antennas Propag.*, vol. 66, no. 6, pp. 3076–3086, Jun. 2018.
[46] K. Zhang, G. A. E. Vandenbosch, and S. Yan, "A novel design approach for compact wearable antennas based on metasurfaces," *IEEE Trans. Biomed. Circuits Syst.*, vol. 14, no. 4, pp. 918–927, Aug. 2020.
[47] R. B. Ibrahim, S. H. S. B. Mohd, H. B. Md. Khir, Mohd. A. B. Zakariya, and H. Daud, "Powering LED from Wi-Fi: A qualitative assessment for rectenna design," in *Proc. 15th Int. Conf. Sci. Techn. Autom. Control Comput. Eng. (STA)*, Dec. 2014, pp. 793–796.
[48] P. Nintanavongsa, U. Muncuk, D. R. Lewis, and K. R. Chowdhury, "Design optimization and implementation for RF energy harvesting circuits," *IEEE J. Emerg. Sel. Topics Circuits Syst.*, vol. 2, no. 1, pp. 24–33, Mar. 2012.
[49] K. K. A. Devi, Md. D. Norashidah, C. K. Chakrabarty, and S. Sadasivam, "Design of an RF-DC conversion circuit for energy harvesting," in *Proc. IEEE Int. Conf. Electron. Design, Syst. Appl. (ICEDSA)*, Nov. 2012, pp. 156–161.
[50] H. P. D. Paz, V. S. D. Silva, R. Diniz, R. Trevisoli, C. E. Capovilla, and I. R. S. Casella, "Temperature analysis of Schottky diodes rectifiers for low-power RF energy harvesting applications," *IEEE Access*, vol. 11, pp. 54122–54132, 2023.
[51] S. A. A. Shah, A. Basir, Y.-H. Lim, and H. Yoo, "A novel efficient wirelessly powered biotelemetric endovascular aortic stent antenna system," *IEEE Trans. Antennas Propag.*, vol. 1, no. 1, pp. 1–16, Jun. 2023.
[52] H. Wang and P. P. Mercier, "Near-zero-power temperature sensing via tunneling currents through complementary metal-oxide-semiconductor transistors," *Sci. Rep.*, vol. 7, no. 1, pp. 1–7, Jun. 2017.
[53] F. Deng, Y. He, B. Li, L. Zhang, X. Wu, Z. Fu, and L. Zuo, "Design of an embedded CMOS temperature sensor for passive RFID tag chips," *Sensors*, vol. 15, no. 5, pp. 11442–11453, May 2015.
[54] J. Lee and S. Cho, "A 1.4-μW 24.9-ppm/°C current reference with process-insensitive temperature compensation in 0.18-μm CMOS," *IEEE J. Solid-State Circuits*, vol. 47, no. 10, pp. 2527–2533, Oct. 2012.
[55] K. Souri, Y. Chae, F. Thus, and K. Makinwa, "12.7 A 0.85 V 600nw all-CMOS temperature sensor with an inaccuracy of±0.4°c (3σ) from- 40 to 125°c," in *IEEE Int. Solid-State Circuits Conf. Dig. Tech. Papers (ISSCC)*, 2014, pp. 222–223.
[56] M. K. Law and A. Bermak, "A 405-nW CMOS temperature sensor based on linear MOS operation," *IEEE Trans. Circuits Syst. II, Exp. Briefs*, vol. 56, no. 12, pp. 891–895, Dec. 2009.
[57] F. Silveira and D. Flandre, *Low Power Analog CMOS for Cardiac Pacemakers: Design and Optimization in Bulk and SOI Technologies*, vol. 758. Cham, Switzerland: Springer, 2004.
[58] L. Turicchia, B. Do Valle, J. L. Bohorquez, W. R. Sanchez, V. Misra, L. Fay, M. Tavakoli, and R. Sarpeshkar, "Ultralow-power electronics for cardiac monitoring," *IEEE Trans. Circuits Syst. I, Reg. Papers*, vol. 57, no. 9, pp. 2279–2290, Sep. 2010.
[59] J. Dieffenderfer, H. Goodell, S. Mills, M. McKnight, S. Yao, F. Lin, E. Beppler, B. Bent, B. Lee, V. Misra, Y. Zhu, O. Oralkan, J. Strohmaier, J. Muth, D. Peden, and A. Bozkurt, "Low-power wearable systems for continuous monitoring of environment and health for chronic respiratory disease," *IEEE J. Biomed. Health Informat.*, vol. 20, no. 5, pp. 1251–1264, Sep. 2016.
[60] Y. Ji, C. Jeon, H. Son, B. Kim, H.-J. Park, and J.-Y. Sim, "A 9.3 nW all-in-one bandgap voltage and current reference circuit using leakage-based PTAT generation and DIBL characteristic," in *Proc. 23rd Asia South Pacific Design Autom. Conf. (ASP-DAC)*, Jan. 2018, pp. 309–310.
[61] J. Salvia, P. Lajevardi, M. Hekmat, and B. Murmann, "A 56Mω CMOS TIA for MEMS applications," in *Proc. IEEE Custom Integr. Circuits Conf.*, Sep. 2009, pp. 199–202.
[62] J. Hu, Y.-B. Kim, and J. Ayers, "A low power 100MO CMOS front-end transimpedance amplifier for biosensing applications," in *Proc. 53rd IEEE Int. Midwest Symp. Circuits Syst.*, Aug. 2010, pp. 541–544.

HUSSEIN YAHYA ALKHALAF received the B.Sc. degree in computer communication engineering from Al-Rafidain University College, Baghdad, Iraq, in 2012, and the M.Eng. degree in communication and computer engineering from the National University of Malaysia (UKM), Bangi, Selangor, Malaysia, in 2019. He is currently a Ph.D. Scholar in biomedical engineering with the University of Malaya (UM), Kuala Lumpur, Malaysia. His research interests include a diverse range of topics across biomedical engineering and related fields, including energy harvesting, rectennas, metamaterials and metasurfaces, wearable antennas, implantable antennas, biosensors, wireless power transfer for biomedical devices, and the development of next-generation wearable technologies for health monitoring.

MOHD YAZED AHMAD (Member, IEEE) received the B.E. degree in electrical engineering from the University of Malaya, Kuala Lumpur, Malaysia, in 2003, the M.Eng.Sc. degree in instrumentation from the Department of Biomedical Engineering, University of Malaya, in 2006, and the Ph.D. degree in electrical engineering science from the University of Technology Sydney, NSW, Australia, in 2013. He is currently a Senior Lecturer with the Department of Biomedical Engineering, Faculty of Engineering, University of Malaya. Previously, he was the Head of the E-Learning Unit at the university level and the Program Coordinator at the faculty level. His research interests include energy harvesting, wireless power transfer, wireless sensing, smart buildings, and intelligent IoT systems, with a particular emphasis on the practical implementation of embedded and cloud-based systems.

HARIKRISHNAN RAMIAH (Senior Member, IEEE) received the B.Eng. (Hons.), M.Sc., and Ph.D. degrees in electrical and electronic engineering from the Universiti Sains Malaysia. His expertise lies in analog and digital IC design. He was with Intel Technology and SiresLabs Sdn. Bhd, specializing in high-frequency signal integrity analysis. Currently, he is a Professor with the Department of Electrical Engineering, University of Malaya, focusing on RF integrated circuit and RF energy harvesting circuit design. He is also the Director of the Center of Research Industry 4.0 (CRI 4.0), University of Malaya. He has published several articles on analog-integrated circuit design, RFIC design, VLSI system design, and RFEH power management module design. He is a member of the Institute of Electronics, Information, and Communication Engineers. He has received the Intel Fellowship Grant Award (2000–2008) and research funding from organizations, such as the Motorola Foundation (2014–2021). He is also a Chartered Engineer and a registered Professional Engineer under the Board of Engineers Malaysia.

A. K. M. ZAKIR HOSSAIN (Member, IEEE) received the B.Sc. degree from the Rajshahi University of Engineering and Technology (RUET), Bangladesh, in 2007, the master's degree in electronics/telecommunications from the University of Gvle, Gvle, Sweden, in 2013, and the Ph.D. degree in engineering from International Islamic University Malaysia (IIUM), Kuala Lumpur, Malaysia, in 2017. He is currently a Senior Lecturer with the Fakulti Teknologi Kejuruteraan Elektrik and Elektronik, Universiti Teknikal Malaysia Melaka (UTeM), Malacca, Malaysia. He was a Postdoctoral Research Fellow with IIUM, from 2018 to 2019. He has authored more than 40 peer-reviewed journal articles and conference papers. His current research interests include microwave passive devices, chipless RFIDs, microwave passive sensors, MIMO antennas, and 5G mobile communication. He is a Certified Engineering Technologist with the Board of Engineers Malaysia (BEM), a member of the International Association of Engineers (IAENG) and the IEEE Society, a Full Member of the Institution of Engineering and Technology (IET), and a Graduate Technologist with the Malaysian Board of Technologists (MBOT). He serves as a reviewer for several reputed journals, including those published by IEEE, Hindawi, MDPI, and others.

S. M. KAYSER AZAM was born in Pabna, Bangladesh. He received the B.Sc. degree in electrical and electronic engineering from Khulna University of Engineering and Technology (KUET), Bangladesh, in 2013, and the M.Sc. (Research) degree in electronics engineering from International Islamic University Malaysia (IIUM), Kuala Lumpur, Malaysia, in 2019. He is currently a Ph.D. Scholar with the Department of Electrical Engineering, University of Malaya (UM), Kuala Lumpur, Malaysia. He was a Power Engineer with Huawei Technologies Bangladesh Ltd., from 2014 to 2016. He has authored or co-authored many articles in reputable journals and conferences. His research interests include antennas, wireless components, sensors, applied electromagnetics, and analog electronics. He has served as a Reviewer for IEEE TRANSACTIONS ON CIRCUITS and SYSTEMS—II: EXPRESS BRIEFS and IEEE ACCESS.

AUNG THIHA received the Ph.D. degree in bio MEMS, with a focus on the micro and nanofabrication of carbon nanosensors for bacterial sensing from the University of Malaya. He is a Research Fellow with the Centre for Innovation in Medical Engineering, University of Malaya. His research interests include the design of new miniaturized in vitro diagnostic sensors and wearable physiological monitoring sensors for ubiquitous biosensing.